Heat can cool near-critical fluids

Daniel Beysens,[1,2,*] Thomas Fröhlich,[3,†] and Yves Garrabos[4]

[1]*ESEME, Laboratoire de Physique et Mécanique des Milieux Hétérogènes, UMR CNRS-ESPCI ParisTech,*
Université Paris 6-7, 10 rue Vauquelin, F-75231 Paris Cedex 5, France
[2]*Service des Basses Températures, UMR-E 9004 CEA/UJF-Grenoble 1, INAC, Grenoble F-38054, France*
[3]*CEA, IRAMIS, Service de Physique de l'Etat Condensé, CEA Saclay F-91191 Gif-sur-Yvette, France*
[4]*ESEME, Institut de Chimie de la Matière Condensée de Bordeaux, UPR 9048 CNRS, Université de Bordeaux,*
87 Avenue du Dr. A. Schweitzer, F-33608 Pessac Cedex, France

We report experiments with very compressible fluids near the liquid-gas critical point. These experiments are performed (i) under microgravity in low Earth orbit by using SF_6 at liquidlike density and (ii) under Earth's gravity with CO_2 at gaslike density. The sample fluid is filled in an interferometer cell with its walls maintained at constant temperature. *In situ* thermistors measure the local fluid temperature. One of the thermistors is also used as a heat source to generate heat pulses. With no gravity-induced fluid convection, the evolution of fluid temperature is governed by the balance of heat flux between the thermal boundary layer of the heat source, which compresses the bulk fluid, and the thermal boundary layer at the wall, which expands it. When heat pulses are applied to the fluid under weak or Earth's gravity, a long thermal transient is observed at the end of the heat pulse where the bulk fluid temperature reaches significantly *below* the initial temperature. This unconventional cooling originates from the fast decompression of the fluid, which is induced by the rapid convectively disappearing hot boundary layer at the heat source, and the persistence of an anomalously thin cold boundary layer convectively induced at the cell wall. This striking phenomenon is observed in a large range of temperature, density, and various thermodynamic conditions. This anomalous cooling effect persists for an appreciable period of time corresponding to the diffusive destruction of the cold boundary layer. We found that the effect is also more pronounced when the free fall acceleration is large. We have analyzed the result by using a simple one-dimensional model with *ad hoc* convective heat losses.

I. INTRODUCTION

Fluids at pressure and temperature above the liquid-gas critical point, called supercritical (SC) fluids, are increasingly utilized in many areas of science and industry. In particular, SC state fluids are used in weightless conditions, where they exhibit liquidlike density while remaining homogenous thus circumventing the problems of gas-liquid interface localization and related interfacial phenomena. Their large density state with gaslike transport properties make those fluids quite unique for hosting very efficient chemical reactions, such as the SC water oxidation process [1–3]. Because of their excellent solvent power, a few SC fluids (e.g., CO_2, water) are used as environmentally safe solvents [4,5]. In the vicinity of the critical point, SC fluids exhibit strong anomalies in their transport and thermodynamic properties. In particular, a number of physical parameters become infinitely large or small. For example, the thermal conductivity λ, the specific heat at constant pressure C_p, constant volume C_V, and the isothermal compressibility K_T diverge, whereas the thermal diffusivity D_T tends to zero [6,7].

These remarkable properties make the fluid very compressible and expandable, and ultimately lead to the adiabatic heating process or "piston effect" (PE) [8–11]. During heating of a fluid near the critical point, a thin diffusive thermal boundary layer expands and pressurizes the bulk fluid, resulting in its very fast adiabatic heating. This "critical speeding up" of the thermalization phenomenon occurring at constant volume conditions shows clear contrast with the well-known "critical slowing down" of the heat diffusion process at constant pressure conditions.

We consider here an experimental configuration closely related to a heat exchanger inside a heated supercritical fluid tank typically used in industrial processes. The fluid sample is confined in a temperature-controlled cylindrical cell (Figs. 1 and 2), which is part of an optical interferometer path (see Ref. [10] for details). Two or three thermistors, depending on the cell, measure the temperature of the fluid sample. One thermistor (TH1) is used to apply a heat pulse in the power range of 10–100 mW. The duration of the pulse can be varied. The density variations are monitored by variations in the interferogram. In a first approximation neglecting the heat losses by the wires, the thermal behavior of the fluid is governed by the balance of heat flux between (i) the heat source, which generates the diffusive hot boundary layer (HBL) that compresses the bulk fluid, and (ii) the heat loss at the thermostat walls, which generates a diffusive cold boundary layer (CBL) that decompresses the bulk fluid. As we see in the following (see also Fig. 3), when convection is allowed by buoyancy, the thickness of the HBL remains nearly the same as without convection. In contrast, the CBL is strikingly thinned under convection, which increases the heat losses appreciably.

When heating stops in the presence of an accelerating fluid, the HBL is convected and disappears very rapidly. The thin convection-induced CBL still provokes a contraction of the

---

*Corresponding author: Present address: PMMH-ESPCI, 10 rue Vauquelin, 75231 Paris, France; daniel.beysens@espci.fr.

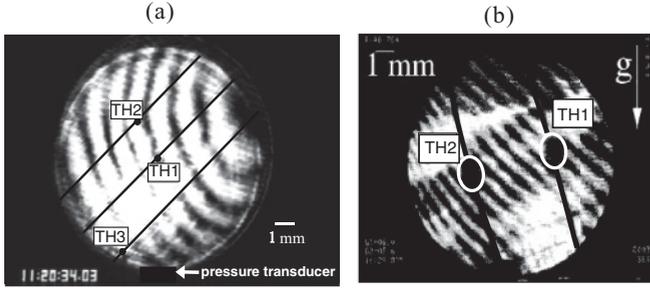†Present address: Astrium GmbH, 81663 Munich, Germany.

FIG. 1. The interferometer cells in a homogeneous state. Thermistors TH1, TH2, and TH3 are denoted by black dots. Their positions are highlighted. TH1 is used for heating. (a) Cell with three 0.25 mm diameter thermistors used in space experiments. (A pressure transducer, not used in this work, is also present). (b) Cell with two 0.89 mm diameter thermistors used in Earth gravity experiments.

fluid volume in its vicinity, resulting in a PE decompression of the sample until the CBL vanishes by diffusion. This fluid decompression is an isentropic process that does not involve a heat flux from the thermostat. As we will see in further details, the pressure drop can also lead to a bulk fluid temperature *below* the thermostat temperature. Although the PE-induced cooling is fast, the phenomenon lasts for an appreciable period of time, corresponding to the diffusive annihilation of the CBL and the development of a negative heat flux at the outer cell walls. During this transient, heating of the fluid could induce temporary cooling, in seemingly apparent violation of the second law of thermodynamics. Wunenburger *et al.* have previously reported similar transient phenomena in a microgravity experiment showing apparent violation of the second principle of thermodynamics in a heated two-phase, gas-liquid sample where the vapor phase was *hotter* than the heated cell wall [12,13]. The present observation also has merit to be observable in laboratory conditions under Earth's gravity.

A full theoretical treatment including hydrodynamics requires sophisticated numerical simulations. A numerical study for a similar case has been performed [14] with CO_2 at critical density. The fluid sample was in a two-dimensional square cavity of 1 cm side length. The fluid was treated as a van der Waals gas. The fluid temperature was initially set at 1 K above
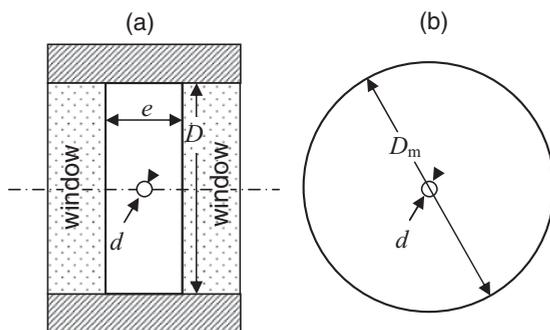

FIG. 2. (a) Schematic cross section (not to scale) of the experimental cylindrical cell (diameter D, thickness e) with its heating thermistor in the center (diameter d). (b) Equivalent spherical model with diameter $D_{mod} = D\sqrt{(1/2)+(e/D)}$ preserving the ratio of heating and cooling surfaces.
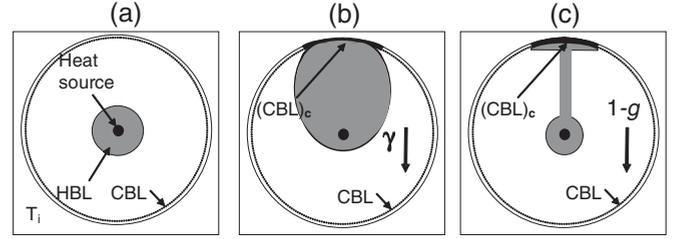

FIG. 3. Schematic of thermal behavior under acceleration for a liquidlike critical fluid confined in a sample at constant temperature $T_i \approx T_c$ (a) $\gamma = 0$. The temperature in the bulk is the result of the balance between a hot PE resulting from the expansion of the HBL and a cold PE, resulting from the contraction of a CBL. (b) $\gamma \neq 0$. The HBL is convected to the wall and the CBL thinners at the zone of contact $[(CBL)_c]$, increasing the cooling effect. (c) $\gamma = 1g$ (Earth gravity acceleration). When heating stops, the HBL is convected from the cell center to the top where it cools down, leading to a pressure and temperature drop that can go below the thermostat temperature.

its critical temperature. The fluid was then heated continuously by a point heat source located at the center with a constant surface heat flux of 0.74 W m^{-1}. This flux level is similar to the heat power of 5 mW dissipated by the thermistor. A plume pattern was developed in the fluid originating from the heat source and reaching to the vertical wall above. The main result is that the forced convection along the thermostated wall enhances the cooling heat flux.

In the following, using a numerical model we describe and analyze two thermalization experiments performed (i) in a SF_6 fluid cell at liquidlike density subjected to a weak acceleration field in the Columbia US Space Shuttle and (ii) in a CO_2 fluid cell at gaslike density subjected to the Earth's gravitational field (noted $1g$). We use a simplified, phenomenological one-dimensional model that considers only the energy equation (see Sec. II below). The convection-induced increase of heat losses with the thermostat is treated as an *ad hoc* cold source. This model explains the data obtained both on ground ($1g$) and in the presence of a small accelerating field, γ, induced by typical maneuvers (rotations and positioning corrections) of the US Space Shuttle (Table I). This controlled acceleration range from $\gamma = 10^{-4}g$ to $10^{-2}g$ ($g = 9.81$ ms^{-2} is the Earth acceleration constant), and its starting and ending time are well identified. The influence of slowly varying acceleration can then be studied in detail, in contrast to the investigation in $1g$, where convection dominates in a very short period of time.

TABLE I. Summary of the different accelerations imposed during the BEM-3 experiment [25]. The amplitudes given for the (1) and (2) rotations correspond to a stationary regime. VRCS: Vernier Rocket Control System; PRCS: Primary Rocket Control System.

Maneuver	Duration	Velocity	Acceleration
(1) rotation	6 min	1 deg/s	23–60 μg
(2) rotation	12 min	1 deg/s	23–60 μg
VRCS firing	0.08 s		300 μg
PRCS firing	0.08 s		30 mg

II. A SIMPLIFIED MODEL

The thermodynamic properties for the critical fluids SF_6 and CO_2 are estimated from a universal scaled form of the equation of state given in Refs. [15,16] with the values of the characteristic parameters issued from Refs. [17–20] in the SF_6 case, and from Ref. [21] in the case of CO_2. The singular (diverging) behavior and regular (background) behavior of the thermal diffusivity D_T and the thermal conductivity λ are well characterized only on the critical isochore (see Refs. [19,20] for SF_6 and Ref. [21] for CO_2). We have noted that the experiments reported here are at a noncritical density (see below for the cell filling conditions). However, quantitative comparison will also be performed relatively far from the critical temperature T_c where the experimental values of D_T and λ can be used with some confidence. A temperature correction $\Delta T_0 = T_c - T_{coex} = T_c[(1/B)(|\rho - \rho_c|/\rho_c)]^{1/\beta}$ is added to account for the temperature difference between the two-phase coexistence temperature T_{coex} and the critical temperature T_c due to the off-critical density difference in each experimental cell. Here ρ (ρ_c) is density (critical density), respectively, B is the value of the coexistence curve amplitude, and β is a critical exponent. We have used the values $B = 1.89$ and $\beta = 0.338$ for SF_6 [22], leading to $\Delta T_0 \approx 0.9$ K for a filling density $\rho \approx 1.27\rho_c$. A similar temperature difference was estimated in the CO_2 case using $B = 2.07$ and $\beta = 0.357$ [23], which corresponds to $\Delta T_0 \approx 0.325$ K for a filling density $\rho \approx 0.82\rho_c$.

We start with the simplified energy conservation equation (at $\gamma = 0$), which was first proposed by Boukari *et al.* [24]. This corresponds to neglect of the spatial variation of pressure and the flow due to the dilatation (or contraction) of the boundary layers during the heating (or cooling) process. For the spherically symmetric case, the equation becomes

$$\frac{\partial T}{\partial t} = \frac{1}{\rho C_p}\frac{1}{r^3}\frac{\partial}{\partial r}\left(r^3\lambda\frac{\partial T}{\partial r}\right) + \left(\frac{\partial T}{\partial p}\right)_S\frac{\partial p}{\partial t} + \frac{\dot{Q}}{mC_p}. \quad (1)$$

Here p is pressure, S is entropy, m is the fluid mass, t is time, and r is the spatial coordinate. $\dot{Q}$ is the heat power source term, sufficient to model the thermal characteristics of the PE dynamics (at a time scale larger than the acoustic time scale) in the absence of gravity and for negligible hydrodynamic velocity.

Then we simulate the convective behavior for the thermal evolution of the fluid under γ acceleration by assuming the following processes (see Fig. 3), which are confirmed by the experiments (see Figs. 4–8):

(i) The diffusive extension of the HBL is weakly affected by convection during heating.

(ii) The HBL is convected by buoyancy toward the cell wall where a thin CBL forms (from the image, it remains on the order of 0.25 mm), increasing the thermal exchange. When coming into contact with the cell wall, the fluid contracts because heat is conducted into the thermostated wall. Heat exchange is thus enhanced when compared to the nonconvection case, leading to pressure and temperature rise lower than that in the absence of an accelerating field.

(iii) When heating stops, the pressure drops due to the thin CBL persisting longer than the pressure rise due to the HBL, which disappears by convection. In order to prevent a diffusive

large extension of the HBL zone and to take the convective loss of hot fluid in this region into account, we introduce an additional negative source term in the energy equation, which acts only in the HBL region:

$$\dot{Q}_{HBL}(r,t) = C[T(r,t) - T_b]. \quad (2)$$

This term—which we name the "convective" heat well—is negative and proportional to the difference between the HBL local temperature $T(r,t)$ and the homogeneous, bulk temperature T_b. The convective amplitude prefactor C (in $W\,K^{-1}$) is phenomenological and accounts for the amplitude of the cooling effect. It has to be determined from the temperature measurements.

Moreover, in order to adapt the above spherical model to the experimental cylinder configuration, we have to preserve the ratio of the heating (thermistor bead) to the cooling (cylindrical body plus plane windows) surfaces (see Fig. 2 for details). As a result, the equal cooling area of the experimental cell and the sphere leads to the sphere diameter $D_{mod} = D\sqrt{(1/2)+(e/D)}$, where D and e are the cell diameter and the cell thickness, respectively. This means that the experimental fluid mass is not preserved in this model, since an equal cooling surface gives $m_{mod}/m_{exp} \approx 1.2$, with m_{exp} the fluid mass in the experimental cylinder and m_{mod} the fluid mass in the model sphere. In a first approximation, for a given amount of energy δQ transferred to the bulk fluid, the amplitude of the PE is inversely proportional to the fluid mass according to [11]

$$\delta T_b = \frac{\delta Q}{m}\left(\frac{1}{C_V} - \frac{1}{C_p}\right). \quad (3)$$

Using this mass ratio, we apply the following correction in the pressure term of the energy conservation of Eq. (1):

$$\left(\frac{\partial T}{\partial p}\right)_S \Rightarrow \frac{m_{mod}}{m_{exp}}\left[\left(\frac{\partial T}{\partial p}\right)_S\right]_{mod}$$
$$= \frac{m_{mod}}{m_{exp}}\left[\left(1 - \frac{C_V}{C_p}\right)\left(\frac{\partial T}{\partial p}\right)_\rho\right]. \quad (4)$$

Here we have made use of the well-known relationship

$$\left(\frac{\partial T}{\partial p}\right)_S = \left(1 - \frac{C_V}{C_p}\right)\left(\frac{\partial T}{\partial p}\right)_\rho. \quad (5)$$

However, a direct application of the mass correction term on the temperature profile during the calculation does not allow the total mass conservation to be preserved in the sample. Therefore, in the first step, the thermalization process is solved according to Eq. (1) and using

$$\frac{dp}{dt} = \frac{\partial p}{\partial t} = -\frac{\int_V\left(\frac{\partial \rho}{\partial T}\right)_p\frac{\partial T}{\partial t}dV}{\int_V\left(\frac{\partial \rho}{\partial p}\right)_T dV} \quad (6)$$

which derives directly from the assumption of uniform pressure and the combination of the total mass conservation of equation

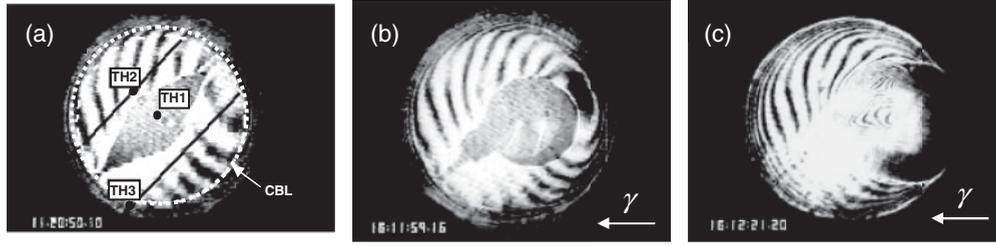$$\int_V\left(\frac{\partial \rho}{\partial t}\right)_p dV = 0, \quad (7)$$

FIG. 4. (a) Development of the hot boundary layer (black, in the center) at the end of a 20 mW, 15 s heat pulse in off-critical ($\rho = 1.27\rho_c$) SF$_6$ at $T_i \approx T_c + 0.05$ K (see text), under zero acceleration. [(b), (c)] About 10 s after the beginning of the heat pulse, the acceleration starts, which drives the hot, expanded fluid toward the cell wall in the opposite direction to TH2 [(b) $t \approx 20$ s; (c) $t \approx 42$ s].

and the expression of the density changes in terms of temperature and pressure variations:

$$d\rho = \left(\frac{\partial \rho}{\partial T}\right)_p dT + \left(\frac{\partial \rho}{\partial p}\right)_T dp. \tag{8}$$

In a second step, the temperature profile is calculated making use of the correction (4). Note that this simple model lowers the true diffusive heat transfer with the cold cell wall because the first calculated profile underestimates the temperature amplitude in the bulk fluid.

According to Ref. [11] the typical diffusion time t_D is calculated over a typical cell length scale $l = V/A = e/2(1 + e/R)$. Here V is the cell volume, A is the cell internal surface area, R (= 6 mm) is the cell radius, and $e \approx 6.7$ mm is the cell thickness. (It follows that $l \approx 1.58$ mm for both cells). It gives

$$t_D = \frac{l^2}{D_T}. \tag{9}$$

The PE time [8,9] follows:

$$t_{\text{PE}} = \frac{t_D}{(\gamma_0 - 1)^2}, \tag{10}$$

with $\gamma_0 = C_p/C_V$.

III. SMALL AMPLITUDE ACCELERATIONS

A. Experiment

We consider the space experiment BEM-3 performed in the Critical Point Facility of European Space Agency onboard the space shuttle Columbia, STS 65 (IML-2, July 1994). Small accelerations are obtained by controlled maneuvers of the spacecraft (see Table I and Ref. [25]). The sample is a cylinder with 12 mm diameter and 6.7 mm thickness, closed by two sapphire windows, as shown in Figs. 1(a) and 2. The fluid is SF$_6$ at liquidlike, off-critical density $\rho \approx 1.27\rho_c$. Three thermistors, labeled TH1, TH2, and TH3, with diameter $d = 0.25$ mm, measure the temperature in three different positions of the cell with a 0.1 mK resolution. TH1 is used to generate a heat pulse of 20 mW electric power whose duration can be varied. The density variations are visualized in the interferometer (for details, see Ref. [26]). Temperature is controlled within 10 μK. The nearest accelerometer to the experiment (Space Acceleration Measurement System SAMS1) was integrated in a Spacelab rack. These measurements were taken at a sampling rate of 25 Hz and filtered by a low-pass filter with

a cut-off frequency of 5 Hz. Further details are described in Ref. [25]. The amplitude γ of the accelerations in the experiment varied roughly between 10^{-4} and $10^{-2}g$. Their duration varied from short firing sequences of the orbiter's VRCS (Vernier Rocket Control System) or PRCS (Primary Rocket Control System) to several minutes when the orbiter rotated. The low amplitudes of an order of $\gamma = 10^{-4}g$, which are given for the orbiter's VRCS and PRCS, correspond to the value at the stationary regime of the acceleration field (Table I). The transient acceleration levels are higher in the beginning and at the end of the maneuvers. We have used the video images to determine the instant when convection sets in as well as its orientation. For the phenomenological analysis carried out below, this criterion is sufficient to support our findings.

B. Observation

We analyze below the case of a heat pulse with 20 mW, 15 s long. The initial fluid temperature is 0.95 K above the coexistence curve temperature T_{coex}, which corresponds to an initial temperature only 50 mK above T_c. Therefore, the sample fluid criticality is here mainly characterized by the liquidlike density distance (+26%) to the critical density along a quasicritical isotherm. The fluid is initially at rest and a HBL develops symmetrically around TH1 and its supplying wires [see Fig. 4(a)]. 10 s after the beginning of heating, the sample is subjected to an acceleration of $3.0 \times 10^{-2}g$. The expanding HBL is driven in the opposite direction of TH2 toward the isothermal sample wall, where it eventually comes into contact [Figs. 4(b) and 4(c)]. The average displacement velocity of the HBL region is approximately 0.5–1 mm/s.

C. Temperature evolution

All three thermistors measure a rapid temperature decrease after heating has ended (Fig. 5). According to the direction of the convective flow (opposite to TH2), the temperature response of TH2 has only a single temperature maximum corresponding to the adiabatic heating amplitude at the end of the heat pulse. In the same figure, the heating thermistor TH1 is seen to relax very quickly after the HBL fluid is convected and the "cold" bulk fluid comes into contact with the thermistor sphere. Surprisingly, the temperature shoots below the initial level T_i. The fastest fluid response is recorded with TH3, whose temperature decreases to $T \leqslant T_i$ within approximately 30 s after the pulse has ended. TH2 and TH1
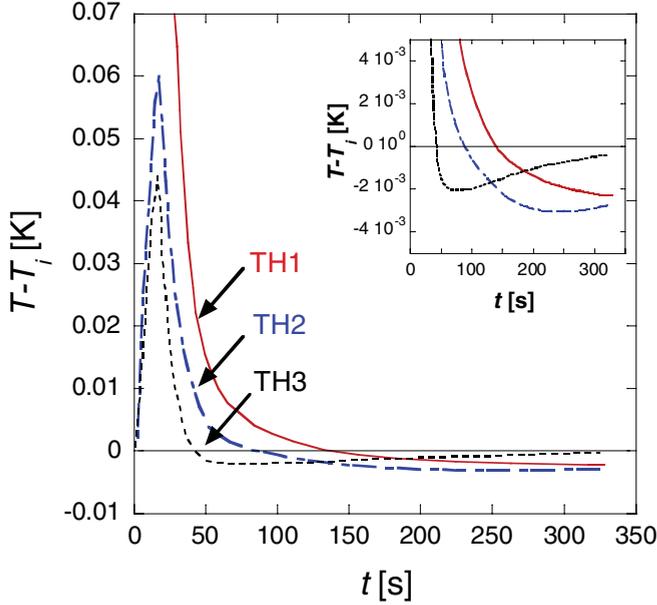
FIG. 5. (Color online) Experimental temperature curves corresponding to the 15 s heat pulse under acceleration as shown in Figs. 3(b) and 3(c). While the cell remains at nearly constant initial temperature (the temperature of the sample housing SCU remains at $T = T_i \approx T_c$), the three thermistors inside the fluid detect a temperature decrease below T_i after the heat pulse has stopped. (The scale is dilated in the inset.)

reach this value at $t \approx 85$ s and $t \approx 150$ s, respectively. After passing through a minimum, all thermistors relax slowly toward T_i. The rapid decrease of the signal recorded by TH3 and the undershoot below T_i is a general feature of the HBL convective displacement: it occurred at every heat pulse with HBL movement.

At this point, a question is raised as to how local temperatures in a system, which receives a certain amount of energy and whose internal energy subsequently increases, can move down (even only for a transient period) below the initial level? A possibility could be that the convected "hot" fluid raises the temperature of the sample housing [called sample cell unit (SCU)] significantly, and that the thermal regulation, whose typical time response is on the order of a few seconds overreacts by an oscillation. This hypothesis does not hold as two thermistors, situated at two different locations inside the SCU, which permanently measure the temperature at a 1 Hz sampling rate, indicate only very small variations $\delta T_{SCU1,2} \leqslant +0.2$ mK during and after the heat pulse.

It is interesting to note that the heating and cooling times are comparable and on the order of the PE time [$t_{PE} \approx 1.3$ s according to (10)]. In contrast, the time to return to the final equilibrium temperature corresponds to the diffusion time $t_D \approx 630$ s [(9)]. It is a clear indication that the cooling process indeed corresponds to an isentropic PE and the return to equilibrium to a diffusive process.

The temperature behavior is then compared with the above simple one-dimensional model (Fig. 6). A good agreement is obtained for TH3 with an amplitude perturbation value $C = 0.006$ W K^{-1} at $t = 10$ s (on the order of the HBL convection time), inducing the characteristic undershoot followed by a
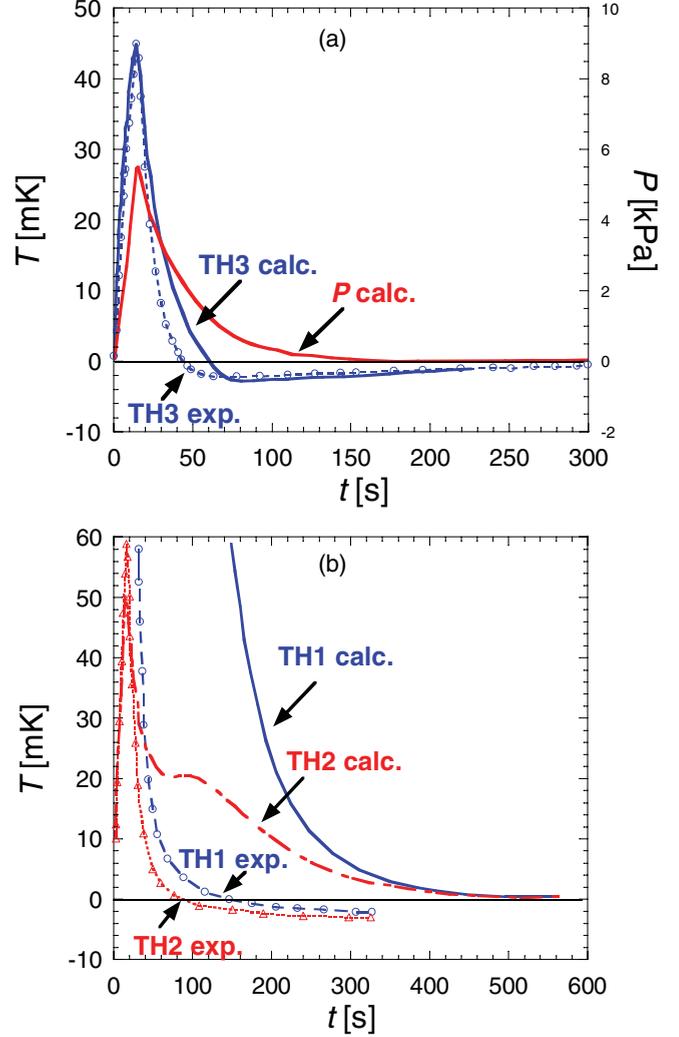

FIG. 6. (Color online) Comparison of experimental (open circles) and calculated (lines) temperature curves and pressure for a 20 mW, 15 s heat pulse in the space experiment under acceleration of Figs. 4(b) and 4(c). In the model, a perturbation of $C = 0.006$ W K^{-1} is imposed at $t \approx 10$ s. In (a) the characteristic undershoot of T_{TH3} near the cell wall and the following slow relaxation is well reproduced whereas in (b) the T_{TH2} (bulk) and T_{TH1} (heat source) relax slower in the model and do not undershoot. This is because in the model the HBL is supposed to remain centered around TH1. The calculated global cell pressure rise $\Delta p = p - p_i$ in (a) also remains above its initial value.

slow relaxation. However, the fast decrease and undershoot of TH1 and TH2 cannot be reproduced by this simple model where the HBL is supposed to remain centered around TH1. As a matter of fact, in the model the global pressure remains above its initial value.

IV. 1g BEHAVIOR

A. Experiment

We now consider a similar sample cell configuration as above, but under a terrestrial environment where a heat source is located in a cylindrical sample of 12 mm diameter and 6.79 mm thickness as described in Fig. 1(b). The fluid is CO_2

at gaslike, off-critical density $\rho = 0.82\rho_c$ [10]. It is the spare cell of the flight cell used in ALICE experiments performed in the Russian Mir Station (see Refs. [10,11] for details). The hot source is a thermistor (TH1) of $d = 0.89$ mm diameter, located 3 mm from the wall. This also works as a thermometer, once heating has stopped. Temperature at the midplane of the bulk fluid is measured by a thermistor (TH2) 3 mm from the wall in the opposite direction with respect to TH1. Temperature measurements are possible only after completion of heating and its resolution is of an order a few mK. The heating power used is 100 mW. Various heat pulses of different duration (40–4000 ms) have been used at various temperatures in the range 200 mK $\leqslant T_i - T_{\text{coex}} \leqslant 16.8$ K. In the following, we focus on the discussion of a case where the effects of a large temperature distance $T_i = T_c + 16.5$ K are combined with a large off criticality (-17%) of the fluid density, resulting in a gaslike nature for the thermodynamic and transport properties.

B. Observation

The position of the thermistors is such that the hot convected fluid does not touch TH2. The evolution of thermal boundary layers during a 100 mW, 4s heat pulse at $T_i = T_{\text{coex}} + 16.5$ K is shown in Fig. 7 (see also the schema in Fig. 3). During the early stages, a thin HBL develops at the thermistor surface and becomes unstable after $t > 200$ ms [Fig. 7(b)]. The layer then remains at a constant thickness of 0.2–0.3 mm and a hot, expanded fluid is convected [Fig. 7(c)], leading to an accumulation of hot fluid in the upper part of the cell. In the regions of the cell that are not perturbed by the convection, a whole shift of the interference fringes shows that density and temperature are homogeneously shifted in the bulk, a key signature of the PE. The large area of contact between the thermostat wall and the convected HBL increases the cold PE, which leads to a pressure and temperature rise in the bulk slower than in the case of no convection. At the beginning of the relaxation period, the HBL is still convected as it is hotter than the bulk, thus accelerating its destruction.
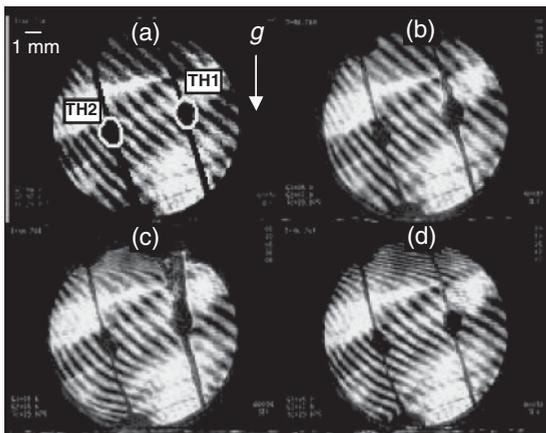

FIG. 7. A 100 mW, 4 s heat pulse in off-critical ($\rho = 0.82\rho_c$) gaslike CO_2 at $T_i \approx T_c + 16.5$ K on Earth. (a) $t = 0$ s, homogeneous state; (b) $t = 240$ ms, onset of convection; (c) $t = 4$ s, end of the heat pulse; (d) $t \approx 10$ s, relaxation.
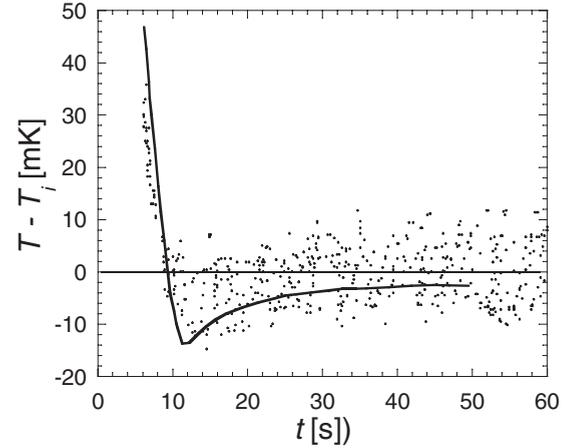

FIG. 8. Time response of thermistor TH2 (dots) during relaxation after a 100 mW, 4 s heat pulse on Earth (TH1 exhibits a similar response). A temperature undershoot below the thermostat temperature is observed. The line is the 1D simulation with $C = 1$ W K^{-1} at $t = 200$ ms in (2) ($T_i = T_c + 16.5$ K).

C. Temperature evolution

Temperature measurements at TH2, after the heat pulse has ended, are shown in Fig. 8. Even though the signal is noisy, one can clearly observe a fast temperature decrease a few seconds after the pulse, which reaches below the set point temperature T_i and reaches a minimum value ($T \approx T_i - 8$ mK) at $t \approx 14$ s. The TH1 temperature evolution (not shown) exhibits a similar evolution. In addition, a 100 mW heat pulse of 1 s duration induces a temperature undershoot of 5–7 mK under similar initial conditions. An influence of the facility's thermal regulation can be excluded on this short time scale.

This temperature behavior can be reasonably described by the one-dimensional (1D) model described above by setting $C = 1$ W K^{-1} at $t = 0.2$ s (on the order of the HBL convection time, Fig. 7). As discussed previously in Sec. III C, it is interesting to note that the heating and cooling times are comparable and on the order of the PE time [$t_{\text{PE}} \approx 17$ s according to (9)], in accord with our model. The time to return to the equilibrium temperature also corresponds well to the diffusion time $t_D \approx 80$ s [(10)].

In Fig. 9 we report the simulation of the spatial evolution of temperature and density. Density decreases near the heat source ($r = 0.445$ mm), shaping the hot boundary layer and increases near the thermostat wall ($r = 6$ mm), determining the cold boundary layer. At short times the CBL is seen as a steep density increase close to the cell wall. Later, its relaxation in the absence of heating provokes the "undershoot" below T_i of the homogeneous bulk temperature, followed by the gradual temperature equilibration. The mass stored in the CBL region is sufficient to compensate not only the density decrease in the HBL region, but it also balances the density decrease of the adiabatic bulk fluid which reaches $\rho_{\text{bulk}} < \rho_i$. Density increase persists near the thermostat wall even after the heat pulse has stopped ($t > 4$ s), depressurizing and cooling the fluid sample until diffusion makes it slowly spread and vanish out.

The isentropic partial derivatives are $(\partial T/\partial p)_S > 0$ and $(\partial T/\partial \rho)_S > 0$. It then follows from the decrease of pressure
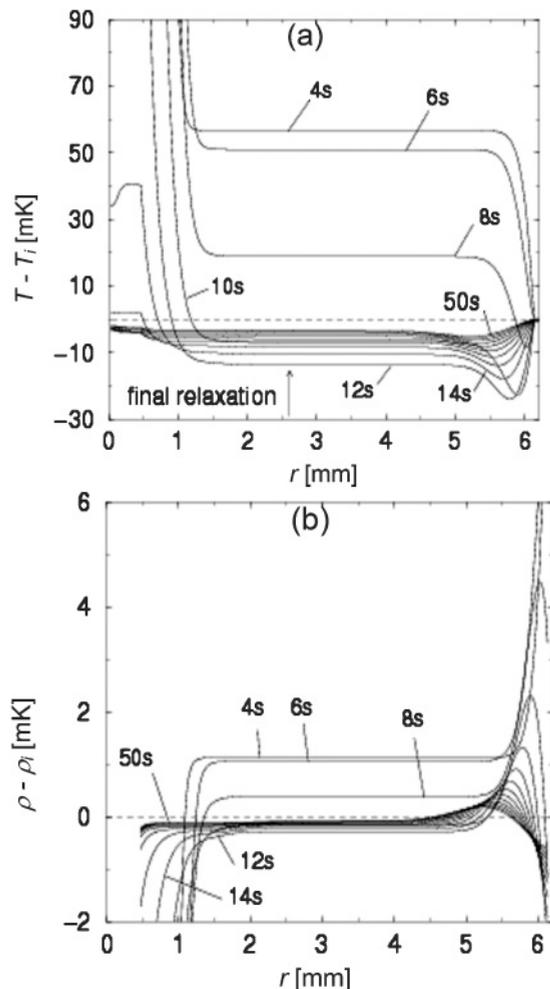
FIG. 9. Calculated relaxation profiles after a heat pulse of 4 s as in Fig. 7 using the 1D model with the approximation of TH1 at the sample center. r is the spatial coordinate. The same strong perturbation as in Fig. 8 ($C = 1\,\mathrm{W\,K^{-1}}$ at $t = 200$ ms) is applied. (a) Evolution of the temperature spatial profile. In the isentropic bulk region, temperature is found to decrease below T_i. (b) Evolution of the density spatial profile. Density decreases near the heat source, shaping the hot boundary layer and increases near the thermostat wall, determining the cold boundary layer. The density increase persists after the heat pulse has stopped ($t > 4$ s), depressurizing and cooling the fluid sample below the initial temperature until diffusion smears it out.

and density of the bulk region to values below the initial state that the global pressure in the cell volume drops below the initial pressure during a transient relaxation phase.

The temperature near the cell wall shows undershoots with a higher amplitude than in the bulk since density is larger at this location. The maximum undershoot occurs at about 12 s, which compares well with the experiment in Fig. 8.

V. CONCLUDING REMARKS

The large compressibility of supercritical fluid near its critical point permits an efficient thermomechanical coupling during the diffusive development of thermal boundary layers. Application of heat flux by an internal heat source in a fluid sample in contact with a thermostat results in a steady state where a hot boundary layer compresses/heats the bulk fluid, and a cold boundary layer decompresses/cools the bulk fluid. When the heating stops, the pressure rise due to the cold layer also stops. However, the pressure drop due to the cold layer still continues as the layer slowly vanishes by diffusion. This results in a temperature drop in the bulk sample that can be reached beyond the initial equilibrium temperature. The effect is more important when the cold boundary layer is thinner, making more efficient heat exchange. This is especially true when the cold boundary layer is convected by buoyancy due to the presence of acceleration. The cooling effect is then more pronounced when the acceleration is larger. As a matter of fact, Earth-based experiments under Earth's terrestrial gravity give a larger cooling than space experiments under acceleration of order $\gamma = 10^{-4}g$. This phenomenon is thus a spectacular demonstration of the thermomechanical nature of the heat exchange by the PE.

A full treatment including hydrodynamics needs more sophisticated numerical simulations [14,27]. Here we have used instead a simple 1D approach that neglects hydrodynamics but accounts for the cooling heat flux by an *ad hoc* coupling parameter. This model provides results in relatively good agreement with the data, with the coupling parameter that varies its value as the sample acceleration, being of an order of 1 for Earth data and 10^{-4} for space data.

We would like to note that the process studied here clearly showed cooling of a supercritical fluid by applying heat pulse. An obvious question can be raised as to whether such a phenomenon could then be used for nonconventional cooling machines.

[1] R. W. Shaw, T. B. Brill, A. A. Clifford, C. A. Eckert, and E. U. Franck, Chem. Eng. News **12**, 26 (1991).

[2] J. W. Tester, H. R. Holgate, F. J. Armellini, P. A. Webley, W. R. Killilea, G. T. Hong, and H. E. Barner, in *Emerging Technologies for Hazardous Waste Management III*, edited by W. D. Tedder and F. G. Pohland, ACS Symposium Series, Vol. 518 (American Chemical Society, Washington, DC, 1993), p. 35.

[3] E. F. Gloyna and L. Li, in *Encyclopedia of Environmental Analysis and Remadiation*, edited by R. A. Meyers (Wiley, New York, 1998), p. 4780.

[4] See, for example, *Supercritical Fluid Technology—Reviews on Modern Theory and Applications*, edited by J. F. Ely and T. Bruno (CRC, Boca Raton, FL, 1991).

[5] P. E. Savage, S. Gopalan, T. I. Mizan, C. J. Martino, and E. E. Brock, AIChE J. **41**, 1723 (1995).

[6] H. E. Stanley, *Introduction to Phase Transitions and Critical Point Phenomena* (Oxford University Press, Oxford, 1971).

[7] M. Barmatz, I. Hahn, J. A. Lipa, and R. V. Duncan, Rev. Mod. Phys. **79**, 1 (2007).

[8] A. Onuki, H. Hao, and R. A. Ferrell, Phys. Rev. A **41**, 2256 (1990); A. Onuki and R. A. Ferrell, Physica A **164**, 245 (1990).

[9] B. Zappoli, D. Bailly, Y. Garrabos, B. Le Neindre, P. Guenoun, and D. Beysens, Phys. Rev. A **41**, 2264 (1990).

[10] M. Bonetti, F. Perrot, D. Beysens, and Y. Garrabos, Phys. Rev. E **49**, R4779 (1994).

[11] Y. Garrabos, M. Bonetti, D. Beysens, F. Perrot, T. Fröhlich, P. Carlès, and B. Zappoli, Phys. Rev. E **57**, 5665 (1998).

[12] R. Wunenburger, Y. Garrabos, C. Lecoutre-Chabot, D. Beysens, and J. Hegseth, Phys. Rev. Lett. **84**, 4100 (2000).

[13] R. Wunenburger, Y. Garrabos, C. Lecoutre, D. Beysens, J. Hegseth, F. Zhong, and M. Barmatz, Int. J. Thermophys. **23**, 103 (2002).

[14] B. Zappoli, A. Jounet, S. Amiroudine, and A. Mojtabi, J. Fluid Mech. **388**, 389 (1999).

[15] Z. Y. Chen, A. Abbaci, S. Tang, and J. V. Sengers, Phys. Rev. A **42**, 4470 (1990).

[16] A. Abacci and J. V. Sengers, An Assessment of the Thermodynamic Properties of Sulfurhexafluoride in the Critical region, University of Maryland Technical Report No. BN 1111, 1990 (unpublished).

[17] W. A. Cole and K. M. de Reuck, Int. J. Thermophys. **11**, 189 (1990); K. M. de Reuck, R. J. B. Craven, and W. A. Cole, IUPAC Thermodynamics Tables Project Center Report, 1991 (unpublished).

[18] C. Guder and W. Wagner, J. Phys. Chem. Ref. Data **28**, 33 (2009).

[19] A. Letaief, R. Tufeu, Y. Garrabos, and B. Le Neindre, J. Chem. Phys. **84**, 921 (1986).

[20] C. Lecoutre, Y. Garrabos, E. Georgin, F. Palencia, and D. Beysens, Int. J. Thermophys. **30**, 810 (2009).

[21] B. Le Neindre, R. Tufeu, P. Bury, and J. V. Sengers, Ber. Bunsenges Phys. Chem. **77**, 262 (1963).

[22] S. N. Biswas, N. J. Trappeniers, and J. H. B. Hoogland, Physica A **126**, 384 (1984); S. N. Biswas and C. A. Ten Seldam, Fluid Phase Equilib. **47**, 67 (1989).

[23] A. Michels, B. Blaisse, and C. Michels, Proc. R. Soc. London, Ser. A **160**, 358 (1937).

[24] H. Boukari, J. N. Shaumeyer, M. E. Briggs, and R. W. Gammon, Phys. Rev. A **41**, 2260 (1990).

[25] M. J. B. Rogers, R. DeLombard, Summary Report of Mission Acceleration Measurements for STS-65, NASA TM-106871, March 1995 (unpublished).

[26] T. Fröhlich, P. Guenoun, M. Bonetti, F. Perrot, D. Beysens, Y. Garrabos, B. Le Neindre, and P. Bravais, Phys. Rev. E **54**, 1544 (1996).

[27] V. S. Nikolayev, A. Dejoan, Y. Garrabos, and D. Beysens, Phys. Rev. E **67**, 061202 (2003).